J. Astrophys. Astr. (1982) **3,** 303–324

Intensity and Polarization Line Profiles in a Semi-Infinite Rayleigh-Scattering Planetary Atmosphere. I. Integrated Flux

R. K. Bhatia and K. D. Abhyankar
Centre of Advanced Study in Astronomy, Osmania University, Hyderabad 500007

Received 1982 April 13; accepted 1982 July 12

Abstract. Absorption and polarization line profiles as well as the curves of growth in the integrated light of a planet over the whole range of phase angles have been computed assuming a semi-infinite atmosphere scattering according to Rayleigh's phase-matrix which takes polarization into account. The relative change in line depth and equivalent widths qualitatively agree with the observations of the CO_2 bands in Venus reported by Young, Schorn and Young (1980). It is pointed out that the bands might be formed in a part of the atmosphere which is different from that where continuum polarization originates.

Key words: Rayleigh scattering—line profiles—atmosphere of Venus

1. Introduction

Efforts to compute line profiles in a scattering planetary atmosphere have been directed towards their computation for the centre of the disk or for some specific points on the disk (Lenoble 1968, 1970; Fymat 1974; Michalsky *et al.* 1974; Teifel 1976; Buriez, Fouquart and Fymat 1979). Attention has also been paid to the study of the variation of equivalent widths with phase angle in the integrated light of the planet (Belton 1968; Whitehill and Hansen 1973; Young and Kattawar 1976; Sato, Kawabata and Hansen 1977). This study is important for knowing the phase function, which determines the nature of the particles, and the structure of the atmosphere (Regas *et al.* 1975; Hunt 1973; Whitehill and Hansen 1973; Kattawar and Young 1977; Anikonov 1977; Buriez and de Bergh 1980). However, there is a lack of a comprehensive coverage of all phase angles for the change in the polarization profile of an absorption line in the integrated light. A few phase angles were covered in the work of Lenoble (1970), Fymat (1974), and Buriez, Fouquart and Fymat (1979). As we shall see, at extreme phase angles, the results obtained are quite different.

We present here results of computations of line profiles and polarization profiles in the integrated light of the planet for the following phase angles: 0, 20, 40, 60, 80, 100, 120, 135, 150 and 175 degrees. We assume a plane-parallel atmosphere with a phase matrix which is realistic for molecular scattering, *viz.* Rayleigh's phase matrix. We have pointed out in a previous paper (Bhatia and Abhyankar 1981) the inadequacy of using Rayleigh's phase function. For Venus, the work of Hansen and Hovenier (1974) based on a Mie-scattering model explained the phase variation of the continuum polarization. In that model, the phase variation of the computed equivalent widths requires that the equivalent widths should show a dip at small phase angles superposed on the general trend in which they first increase with increasing phase angle up to a phase angle of about 80° and then decrease again. However, Young, Schorn and Young (1980) find that the CO_2 bands at 7820, 7883 and 8689 Å do not exhibit such a dip at small phase angles. This has rekindled interest in Rayleigh-scattering models.

2. Basic theory

2.1 *Radiative Transfer*

Let unpolarized radiation of flux $\pi \mathcal{F}$ be incident on a plane-parallel atmosphere in the direction ($\mu_0 = \cos\theta_0, \varphi_0$), θ and φ being spherical coordinates. Then $\mathcal{F}_l = \mathcal{F}_r = \frac{1}{2}\mathcal{F}$, where $\pi\mathcal{F}_l$ and $\pi\mathcal{F}_r$ are the fluxes in two mutually perpendicular directions l and r, parallel and perpendicular to the meridian plane defined by the incident ray (Chandrasekhar 1960). The three components I_l, I_r and U of the scattered radiation I in the direction (μ, φ), where l and r are now the directions parallel and perpendicular to the meridian plane defined by the scattered ray, are given by (Chandrasekhar 1960, p. 259; Lenoble 1970; Abhyankar and Fymat 1971)

$$\mathbf{I}(\mu, \varphi) = \begin{bmatrix} I_l \\ I_r \\ U \end{bmatrix} = \frac{1}{4\mu}\tilde{Q}\tilde{S}(\mu, \varphi, \mu_0, \varphi_0) \begin{bmatrix} \mathcal{F}/2 \\ \mathcal{F}/2 \\ 0 \end{bmatrix}, \tag{1}$$

where

$$\begin{aligned}\left(\frac{1}{\mu}+\frac{1}{\mu_0}\right)\tilde{S}(\mu, \varphi, \mu_0, \varphi_0) &= \tfrac{3}{4}\tilde{\omega}_0 \begin{bmatrix} L_1(\mu) & L_2(\mu) \\ L_3(\mu) & L_4(\mu) \end{bmatrix}\begin{bmatrix} L_1(\mu_0) & L_3(\mu_0) \\ L_2(\mu_0) & L_4(\mu_0) \end{bmatrix} \\ &+ \tfrac{3}{4}\tilde{\omega}_0 (1-\mu^2)^{\frac{1}{2}}(1-\mu_0^2)^{\frac{1}{2}} H^{(1)}(\mu) H^{(1)}(\mu_0) \\ &\times \begin{bmatrix} -4\mu\mu_0\cos(\varphi_0-\varphi) & 0 & 2\mu\sin(\varphi_0-\varphi) \\ 0 & 0 & 0 \\ 2\mu_0\sin(\varphi_0-\varphi) & 0 & \cos(\varphi_0-\varphi) \end{bmatrix} \\ &+ \tfrac{3}{4}\tilde{\omega}_0 H^{(2)}(\mu) H^{(2)}(\mu_0) \\ \times \begin{bmatrix} \mu^2\mu_0^2\cos 2(\varphi_0-\varphi) & -\mu^2\cos 2(\varphi_0-\varphi) & -\mu^2\mu_0\sin 2(\varphi_0-\varphi) \\ -\mu_0^2\cos 2(\varphi_0-\varphi) & \cos 2(\varphi_0-\varphi) & \mu_0\sin 2(\varphi_0-\varphi) \\ -\mu\mu_0^2\sin 2(\varphi_0-\varphi) & \mu\sin 2(\varphi_0-\varphi) & -\mu\mu_0\cos 2(\varphi_0-\varphi) \end{bmatrix},\end{aligned} \tag{2}$$

$$\tilde{Q} = \begin{bmatrix} 1 & 0 & 0 \\ 0 & 1 & 0 \\ 0 & 0 & 2 \end{bmatrix}, \tag{3}$$

and

$$\tilde{L}(\mu) = \tilde{M}(\mu) \cdot \tilde{H}(\mu) . \tag{4}$$

Here

$$\tilde{M}(\mu) = \begin{bmatrix} \mu^2 & (1-\mu_0^2)\sqrt{2} \\ 1 & 0 \end{bmatrix} \tag{5}$$

and

$$\tilde{H}(\mu) = \begin{bmatrix} H_1 & H_2 \\ H_3 & H_4 \end{bmatrix} \tag{6}$$

is defined by

$$\tilde{H}(\mu) = \tilde{E} + \mu \tilde{H}(\mu) \int_0^1 \frac{\tilde{H}^{\mathrm{tr}}(\mu') \tilde{\Psi}(\mu') d\mu'}{\mu + \mu'}, \tag{7}$$

where E is the unit matrix, 'tr' denotes transpose, and the characteristic matrix $\tilde{\psi}(\mu)$ is given by

$$\tilde{\Psi}(\mu) = \tfrac{3}{8} \tilde{\omega}_0 \tilde{M}^{\mathrm{tr}}(\mu) \cdot \tilde{M}(\mu). \tag{8}$$

The matrix $\tilde{H}$ is related to the matrix $\tilde{N}$ defined by Abhyankar and Fymat (1971) as

$$\tilde{N}(\mu) = \tfrac{1}{2} \sqrt{3}\, \tilde{M}(\mu) \cdot \tilde{H}(\mu). \tag{9}$$

The functions $H^{(1)}(\mu)$ and $H^{(2)}(\mu)$ are obtained from

$$H^{(n)}(\mu) = 1 + \mu H^{(n)}(\mu) \int_0^1 \frac{\Psi^{(n)}(\mu') H^{(n)}(\mu') d\mu'}{\mu + \mu'}, \quad (n = 1, 2) \tag{10}$$

where the characteristic functions $\psi^{(1)}(\mu)$ and $\psi^{(2)}(\mu)$ are given by $\frac{3}{8} \tilde{\omega}_0(1 + 2\mu^2)(1 - \mu^2)$ and $\frac{3}{16} \tilde{\omega}_0(1 + \mu^2)^2$, respectively. Here $\tilde{\omega}_0 \in (0, 1)$ is the is the single scattering albedo. We have, therefore,

$$\begin{aligned} I_i(\mu, \varphi) = \tfrac{3}{32} \frac{\mu_0 \tilde{\omega}_0}{\mu + \mu_0} \{ & L_1(\mu) [L_1(\mu_0) + L_3(\mu_0)] + L_2(\mu) [L_2(\mu_0) + L_4(\mu_0)] \\ & - 4 \mu\mu_0 (1-\mu^2)^{\frac{1}{2}} (1-\mu_0^2)^{\frac{1}{2}} H^{(1)}(\mu) H^{(1)}(\mu_0) \cos(\varphi_0 - \varphi) \\ & + \mu^2 (\mu_0^2 - 1) H^{(2)}(\mu) H^{(2)}(\mu_0) \cos 2(\varphi_0 - \varphi) \} \mathcal{F}, \end{aligned} \tag{11}$$

$$I_r(\mu, \varphi) = \tfrac{3}{32} \frac{\mu_0 \tilde{\omega}_0}{\mu + \mu_0} \{L_3(\mu)\,[L_1(\mu_0) + L_3(\mu_0)] + L_4(\mu)\,[L_2(\mu_0) + L_4(\mu_0)]$$

$$- (\mu_0^2 - 1)\, H^{(2)}(\mu)\, H^{(2)}(\mu_0) \cos 2(\varphi_0 - \varphi)\}\, \mathcal{F}, \tag{12}$$

$$U(\mu, \varphi) = \tfrac{3}{16} \frac{\mu_0 \tilde{\omega}_0}{\mu + \mu_0} \{2\mu_0 (1 - \mu^2)^{\frac{1}{2}} (1 - \mu_0^2)^{\frac{1}{2}} \sin(\varphi_0 - \varphi)\, H^{(1)}(\mu)\, H^{(1)}(\mu_0)$$

$$- \mu (\mu_0^2 - 1) \sin 2(\varphi_0 - \varphi)\, H^{(2)}(\mu)\, H^{(2)}(\mu_0)\}\, \mathcal{F}. \tag{13}$$

$I = I_l + I_r$ gives the total intensity. Further, in terms of the Stokes parameters, the degree of linear polarization is given by

$$\sigma = \frac{[(I_l - I_r)^2 + U^2]^{\frac{1}{2}}}{I_l + I_r}. \tag{14}$$

It should be noted that one can write $\sigma = -Q/I$ if and only if $U = 0$; but in general $U \neq 0$. Also, polarization is a positive quantity (*cf.* Clarke 1974) and mention of negative polarization should be avoided. Instead, the fact can be stated as: the *l*-component becomes larger than the *r*-component. In planetary studies, the definition $\sigma = -Q/I$ is used because it is found observationally that the electric vector for the integrated flux lies either along the equator or perpendicular to it (Dollfus 1961), which implies that $U = 0$ in that case.

2.2 *The Line Profile*

We assume a Lorentz line profile for absorption in the line, which holds at high pressures. In terms of the absorption coefficient k_0 at the line centre, the absorption coefficient k at any frequency ν is given by

$$k = k_0 \{[1 + ((\nu - \nu_0)/\alpha_L)^2]\}^{-1} \tag{15}$$

where $\alpha_L = \alpha_0\, p$ is the Lorentz half-width of the line at pressure p expressed in units of the standard pressure. It is more convenient to express the line profile in terms of the albedo $\tilde{\omega}_\nu$, given by

$$\tilde{\omega}_\nu = \frac{\sigma}{\sigma + k_\nu} \tag{16}$$

where σ is the scattering coefficient assumed to be independent of frequency over the line.

If k_c is the absorption coefficient in the continuum, the monochromatic albedo will be

$$\tilde{\omega}'_\nu = \frac{\sigma}{\sigma + k_\nu + k_c}. \tag{17}$$

Then

$$\tilde{\omega}'_\nu = \left[\frac{1}{\tilde{\omega}_\nu} + \frac{1}{\tilde{\omega}_c} - 1\right]^{-1},$$

or

$$\tilde{\omega}'_\nu = \left[\frac{1-\tilde{\omega}_0}{\tilde{\omega}_0\,(1+x^2)} + \frac{1}{\tilde{\omega}_c}\right]^{-1} \tag{18}$$

where

$$x = (\nu - \nu_0)/\alpha_L. \tag{19}$$

2.3 *Equivalent Width*

Equivalent width is a measure of the radiation depletion produced by the line and is given by

$$W = \int_{\text{line}} (1 - I_\nu/I_c)\, d\nu$$

And (20)

$$W = \int_{\text{line}} (1 - F_\nu/F_c)\, d\nu$$

in terms of intensity and flux respectively. Here the subscript 'c' denotes the continuum, while I and F represent the total intensity in both states of polarization. We can similarly define the equivalent width for intensity or flux for the two components in any two perpendicular directions, separately.

2.4 *The Curve of Growth*

In a non-scattering atmosphere, the variation of the equivalent width with the number of absorbing particles gives the curve of growth. The analogue of the number of absorbing particles in a scattering atmosphere is the specific abundance. We have chosen for the abscissa of the curve of growth the quantity $[(1/\tilde{\omega}_0) - 1] = S/\pi\alpha_L\sigma$ which is proportional to the line strength, S. Here $\tilde{\omega}_0$ is the albedo at line centre without continuum absorption. This definition differs from that used by Chamberlain (1978) by a factor $\tilde{\omega}_c$, the continuum albedo, in the numerator: $S\,\tilde{\omega}_c/\pi\alpha_L\sigma$.

3. Computation of integrated flux

We use Horak's (1950) method to compute the flux. Consider any point A on the planet (see Fig. l). This point can be represented in two different coordinate systems:

(i) the usual spherical coordinates (μ = cos θ, φ), and (ii) the planetary coordinate system. In the first case a rectangular coordinate system is set up at point A with the z-axis in the radial direction and x-axis in the horizontal plane in such a way that the azimuthal angle of the incoming ray is zero. The second system is represented by the planetary longitude η and the colatitude β which are defined with respect to the intensity equator and the meridian. The direction cosine of the incident ray μ_0, the direction cosine of the scattered ray μ and its azimuthal angle φ are given in terms of the phase angle α, by

$$\mu_0 = \sin\beta \cos(\eta - \alpha), \tag{21}$$

$$\mu = \sin\beta \cos\eta, \tag{22}$$

$$\cos\varphi = \frac{\mu\mu_0 - \cos\alpha}{(1-\mu^2)^{1/2}(1-\mu_0^2)^{1/2}} \tag{23}$$

and

$$\sin\varphi = \frac{\sin\alpha\cos\beta}{(1-\mu^2)^{1/2}(1-\mu_0^2)^{1/2}}. \tag{24}$$

For a particular phase angle α , the flux at earth is given by

$$F' = \frac{1}{D^2}\int\int I(\theta, \varphi)\,\mu dA \tag{25}$$

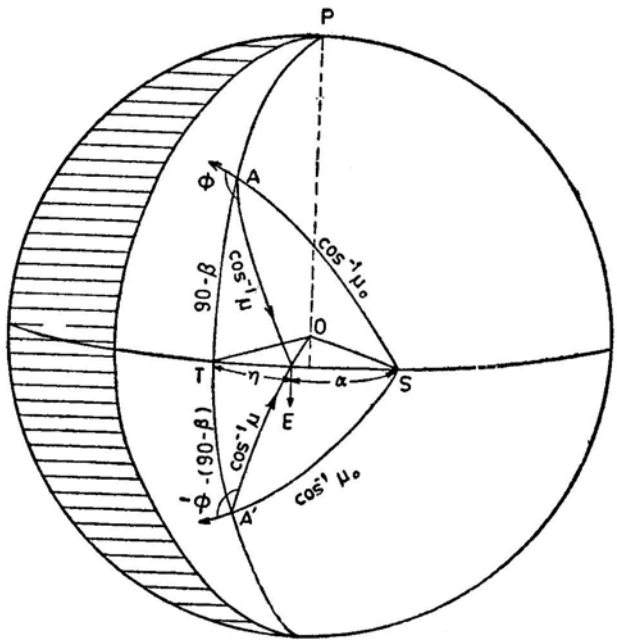

Figure 1. Geometry of scattering for a point on the disk of the planet at a phase angle α.

where D = distance of the planet from the earth and $dA = r^2 \sin\beta\, d\beta\, d\eta$ is an element of area, r being the radius of the planet. The integration is performed over the visible planetary disk. Substituting the values of μ and dA we have

$$F' = (r/D)^2 \int_0^{\pi} \int_{\alpha-\pi/2}^{\pi/2} I(\beta, \eta) \sin^2\beta d\beta \cos\eta\, d\eta. \tag{26}$$

Since (r/D) is a constant, we have

$$F = F'/(r/D)^2 = \int_0^{\pi} \int_{\alpha-\pi/2}^{\pi/2} I(\beta, \eta) \sin^2\beta d\beta \cos\eta\, d\eta. \tag{27}$$

Any one of the various numerical methods can be used to evaluate the double integral. The most efficient method is that of Chebycheff–Gauss quadrature. The necessary transformation equations and weights and divisions are given by Horak (1950). We have then

$$F = \tfrac{1}{2}(1 + \cos\alpha) \sum_i \sum_j a_i\, b_j\, I(\psi_i, \xi_j) \tag{28}$$

where a_i and b_j are the weights and ψ_i and ξ_j the divisions for β and η respectively. We have used a 36-point grid for quadrature. The integral can be evaluated for one hemisphere and the total flux can be obtained by doubling the result.

The above discussion is valid for the total intensity I which is independent of the coordinate frame chosen. However, for computing the integrated flux for the Stokes components, two additional factors have to be taken into consideration:

(i) The Stokes parameters I_l and I_r calculated from Equations (11) and (12) for a given point characterized by μ, μ_0 and φ are respectively parallel and perpendicular to the meridian plane of the scattered ray defined in the coordinate system set up at that point. In Fig. 1 the arc AE defines this meridian plane at point A. Therefore, before performing the integration over the disk, these parameters have to be referred to a common coordinate system. As is customary and convenient for observations we choose the two axes to be parallel and perpendicular to the intensity equator.

(ii) The sign of the azimuthal angle φ will be different in the two hemispheres; while this will not affect I_l and I_r, the parameter U will have opposite signs at the corresponding points in the two hemispheres (*cf.* Equations 11–13).

The new Stokes parameters, which we will differentiate from the original set by the superscript e, can be obtained by the transformation

$$\begin{bmatrix} I_l^e \\ I_r^e \\ U^e \end{bmatrix} = \begin{bmatrix} \cos^2 i & \sin^2 i & \tfrac{1}{2}\sin 2i \\ \sin^2 i & \cos^2 i & -\tfrac{1}{2}\sin 2i \\ -\sin 2i & \sin 2i & \cos 2i \end{bmatrix} \begin{bmatrix} I_l \\ I_r \\ U \end{bmatrix}, \tag{29}$$

where i, the angle between the meridian plane containing the direction (μ, φ) of the scattered ray and the equator, is given by

$$\cos i = (\sin\beta - \mu \cos\eta)/(1 - \mu^2)^{\frac{1}{2}} \sin\eta.$$

In the northern hemisphere the transformation is applied clockwise and i is positive. However, for the corresponding point in the southern hemisphere with the same μ and μ_0 the transformation matrix has to be applied counter-clockwise ; in addition although the magnitude of φ is the same, its sign is negative (*cf.* point A' in Fig. 1). One therefore obtains the following expressions for the Stokes parameters for the northern and southern hemispheres.

$$I_l(N) = (\cos^2 i)I_l + (\sin^2 i)I_r + (\tfrac{1}{2}\sin 2i)U,$$

$$I_r^e(N) = (\sin^2 i)I_l + (\cos^2 i)I_r - (\tfrac{1}{2}\sin 2i)U,$$

$$U^e(N) = \sin 2i\,(I_r - I_l) + (\cos 2i)U \tag{30}$$

and

$$I_l^e(S) = I_l^e(N),$$

$$I_r^e(S) = I_r^e(N),$$

$$U^e(S) = -U^e(N). \tag{31}$$

Adding Equations (30) and (31), we get the following expressions for the combined result for the two points:

$$I_l^e = 2[(\cos^2 i)I_l + (\sin^2 i)I_r + (\tfrac{1}{2}\sin 2i)U],$$

$$I_r^e = 2[(\sin^2 i)I_l + (\cos^2 i)I_r - (\tfrac{1}{2}\sin 2i)U],$$

$$U^e = 0. \tag{32}$$

With these expresions, after performing the integration over the disk, the degree of polarization given by Equation (13) becomes

$$\sigma = (F_r^e - F_l^e)/(F_r^e + F_l^e) \tag{33}$$

showing that we are justified in taking $\sigma = -Q/I$, as $U = 0$ for the integrated flux.

Using Equations (11), (12), (13), (32), (33) and (28) with the H-functions given by Abhyankar and Fymat (1971) the fluxes F_l^e, F_r^e, $F = F_l^e + F_r^e$ and the degree of polarization σ were calculated for various albedos at different phase angles. These results are presented and discussed below.

4. The line profiles in F_l^e, F_r^e and F

4.1 *General Behaviour*

For the total flux F, the absorption profiles for three line strengths $\tilde{\omega}_0 = 0{\cdot}2$, $0{\cdot}6$ and $0{\cdot}9$ are shown in Figs 2, 3 and 4, respectively. In all the three cases, these curves

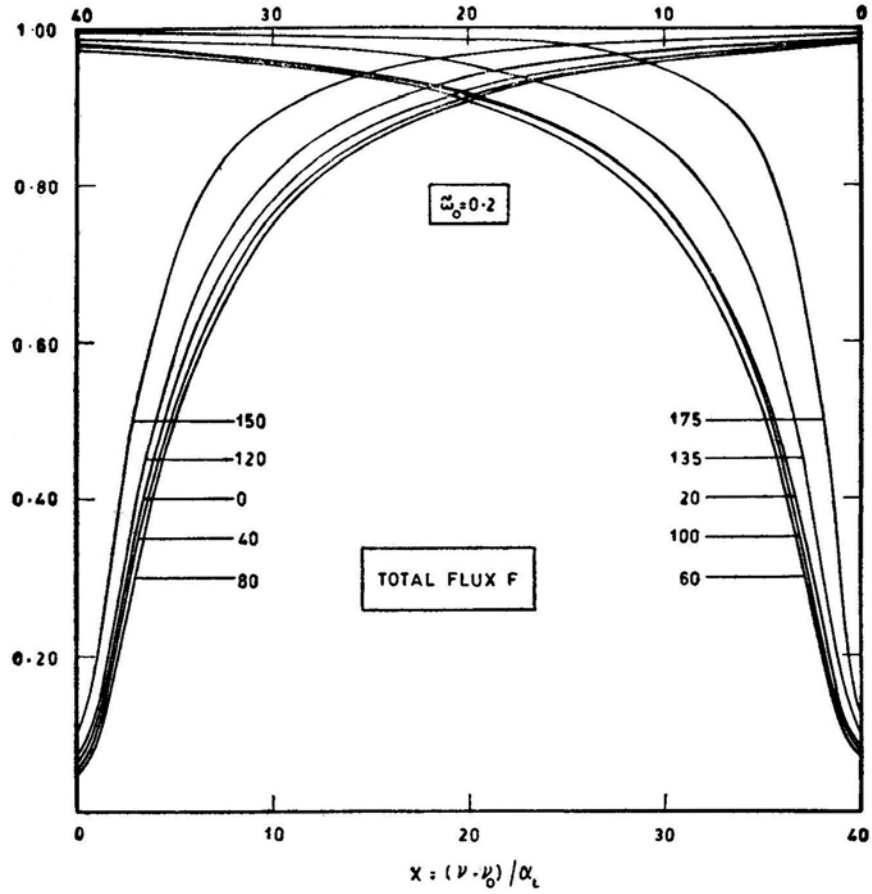

Figure 2. Line profiles for the total flux F in the case of a strong line with $\tilde{\omega}_0 = 0{\cdot}2$ at different phase angles.

point to an increase in absorption with phase angle up to about 90° and then a decrease. Further, we note that the absorption profile in the inner part of the line at phase angle 20° is slightly lower than at phase angle 100°, but in the outer part the profile is higher; there is no such crossover in other cases.

Figs 5 and 6 show the F_l^e and F_r^e profiles for $\tilde{\omega}_0 = 0{\cdot}2$. It may be noted from Fig. 6 that the F_r^e line becomes monotonically weaker with increasing phase angle. On the other hand Fig. 5 shows that the F_l^e line shows first an increase in strength and then a decrease. Further, the change in the F_l^e profile with phase angle is evidently much more pronounced than that in the F_r^e profile. This can be explained as follows. The F_r^e component, being perpendicular to the scattering plane, is scattered isotropically while the F_l^e component, being parallel to the scattering plane, has the $\cos^2 \Theta = \cos^2 \alpha$ dependence, $\Theta = 180 - \alpha$ being the scattering angle. The behaviour of the lines of other strengths ($\tilde{\omega}_0 = 0{\cdot}6$ and $0{\cdot}9$) is essentially similar, except that the changes become more pronounced as the line becomes weaker with increasing value of $\tilde{\omega}_0$. The effects of changing the continuum albedo are shown in Fig. 7 for a line of strength $\tilde{\omega}_0 = 0{\cdot}6$. It is seen that the lines become stronger for $\tilde{\omega}_c = 0{\cdot}997$

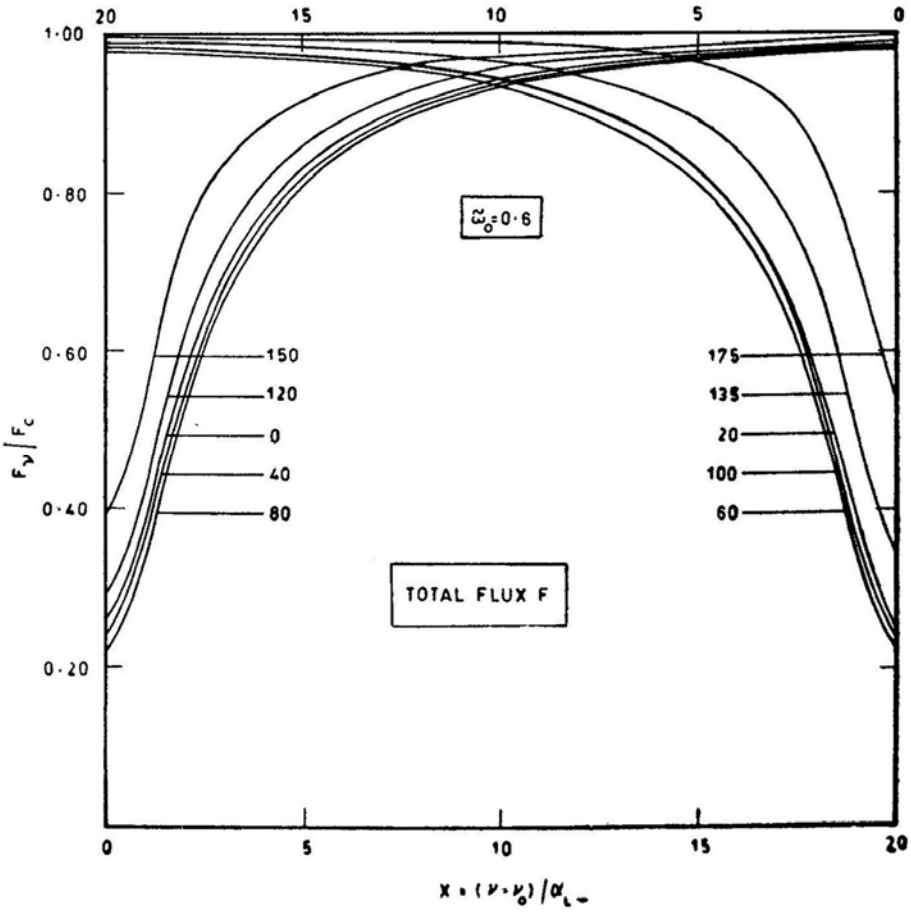

Figure 3. Line profiles for the total flux F in the case of a strong line with $\tilde{\omega}_0 = 0{\cdot}6$ at different phase angles. Note the change in the scale of the abscissa compared with Fig, 2.

as compared with $\tilde{\omega}_c = 0{\cdot}99$, both the line centre and wings being lower in the former case. This effect also becomes more pronounced for weak lines.

4.2 *Line Depth*

The change in line depth R_0 defined by $(1 - Zv_0/Z_c)$, $(Z = F, F_l^e, F_r^e)$, with phase angle is shown in Fig. 8 for $\tilde{\omega}_0 = 0{\cdot}9$. We note that for the F_r^e component there is an almost monotonic decrease while F_l^e and F first show an increase and then a decrease which has been noted above. These changes are small for a strong line and become more pronounced as the line becomes weaker. However, observations of weak lines are difficult, one of the major problems being the delineation of the continuum. Line-depth ratios can be obtained photometrically quite accurately and fast.

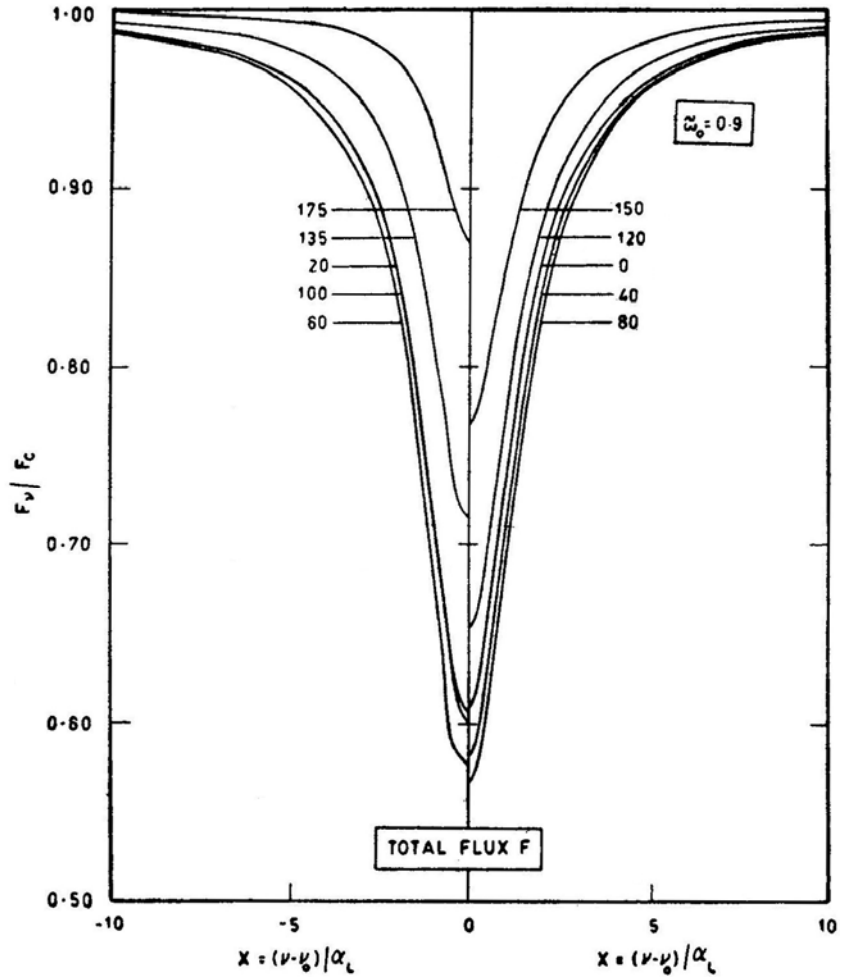

Figure 4. Line profiles for the total flux F in the case of a strong line with $\tilde{\omega}_0 = 0{\cdot}9$ at different phase angles. Note the change in the scale compared with Figs 2 and 3.

5. Equivalent widths and curves of growth

5.1 *The Equivalent Widths*

The variation of relative equivalent width with phase angle is shown in Fig. 9 for three cases: $\tilde{\omega}_0 = 0{\cdot}1$, $0{\cdot}9$, and $0{\cdot}9999$. The long-dashed curve is for the F_l^e component, the short-dashed one for the F_r^e component and the full curve for the total flux F. Two features are prominently seen in these figures: (i) The F_r^e component shows a continuous decrease with increasing phase angle while the F_l^e component shows an increase up to $\alpha = 90°$ and then a decrease. Further, the variation in equivalent width is much larger in F_l^e than in F_r^e and (ii) the change shown by all three curves is a function of line strength, the weakest line exhibiting the maximum change.

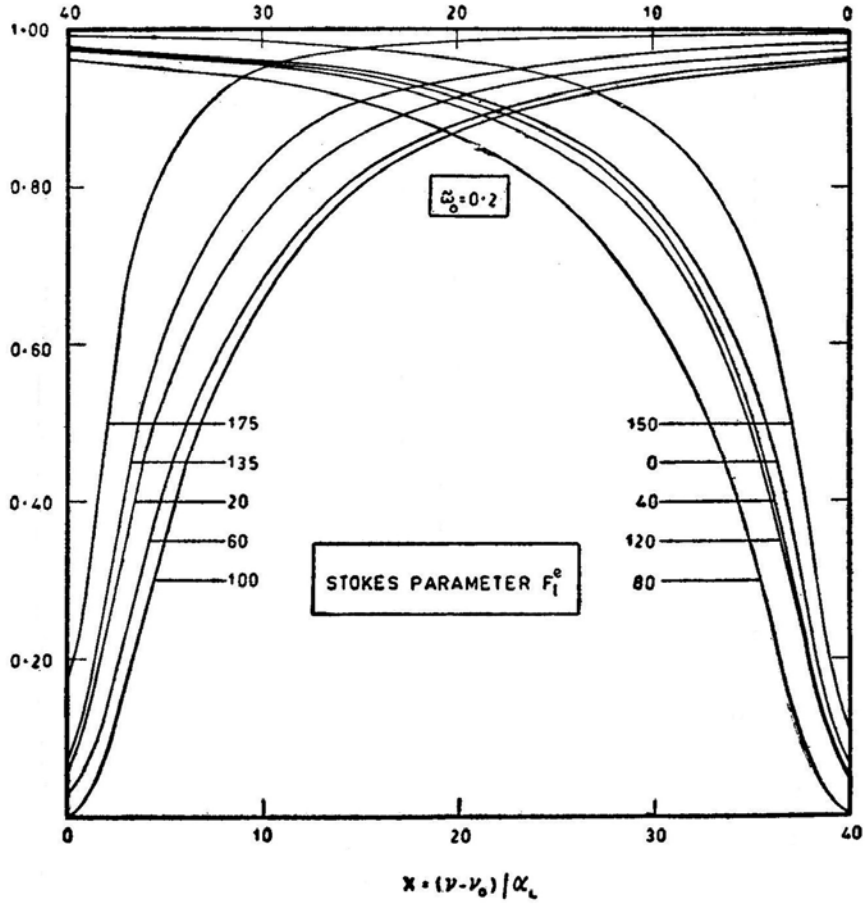

Figure 5. Line profiles for the Stokes' parameter F_l^e in the case of a strong line with $\tilde{\omega}_0 = 0{\cdot}2$ at different phase angles.

The first, fact has already been explained: the F_r^e component is scattered isotropically while the F_l^e component is Scattered according to $\cos^2 \Theta$. Thus, it is to be expected that the phase variation of the F_r^e component should agree with that computed for the total flux F for an atmosphere scattering isotropically. This indeed is the case (see *e.g.* Chamberlain 1978 p. 139; Lestrade and Chamberlain 1978).

Observations for the CO_2 bands in Venus do show that the equivalent widths first increase with phase angle and then decrease (Young 1972; Barker and Macy 1977; Macy and Trafton 1977). Consequently, a homogeneous atmosphere scattering isotropically is ruled out because as noted above, it predicts a monotonic decrease of equivalent widths with phase angle (see also Chamberlain 1970). Hunt (1972) has argued for a two-layer atmosphere to explain this effect while Regas *et al.* (1973) disagree and emphasize that a two-layer model is not necessary (see also Kattawar and Young 1977). Whitehill and Hansen (1973) and Barker and Macy (1977) have investigated this effect taking Mie scattering into account for a single-layer atmosphere. However, this requires an additional dip in equivalent widths at very small phase angles, between 0° and 10°. Schorn, Young and Young (1979) comment: 'We conclude that the 8689 Å data suggest a rather uncertain decrease of the order

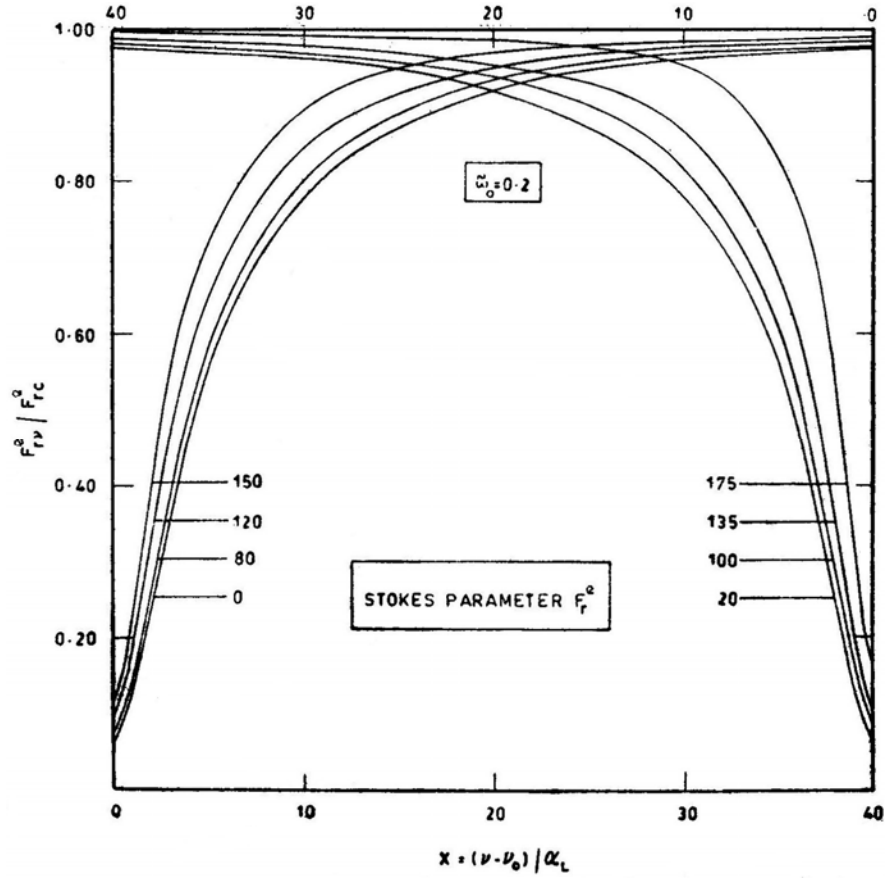

Figure 6. Line profiles for the Stokes' parameter F_r^Q in the case of a strong line with $\tilde{\omega}_0 = 0{\cdot}2$ at different phase angles. The profiles for phase angles 40° and 60° (not shown) are very close to those at 0° and 20° , respectively.

of 10 per cent in equivalent width at small phase angles'. In a later paper, Young, Schorn and Young (1980) have analysed the observations of the 7820, 7883 and 8689 A bands from 1967 to 1975 in which there was no indication of a dip at small phase angles in any of the three bands. But all of them show first an increase in equivalent width with increasing phase angle up to about 80° and then a decrease at larger phase angles. This so-called inverse phase effect becomes more pronounced as we go from stronger to weaker lines which is exactly what we see in Fig. 9 for a Rayleigh scattering atmosphere. It appears that the region where the bands are formed is different from the level in the atmosphere where continuum polarization requiring Mie scattering is produced. As discussed by us elsewhere (Bhatia and Abhyankar 1982) the total phase matrix can be represented as a sum $\tilde{P} = a\tilde{R} + (1 - a)\,\tilde{M}$ where $\tilde{R}$ and $\tilde{M}$ stand for Rayleigh and Mie phase matrices, respectively and the weight a varies from unity at the top of the atmosphere to zero as we go deeper into the atmosphere, at a rate characteristic of the relative scale heights of the aerosols and gas molecules.

The dependence of phase effect on line strength can be understood from the concept of the effective depth of line formation (Lestrade and Chamberlain 1980). As

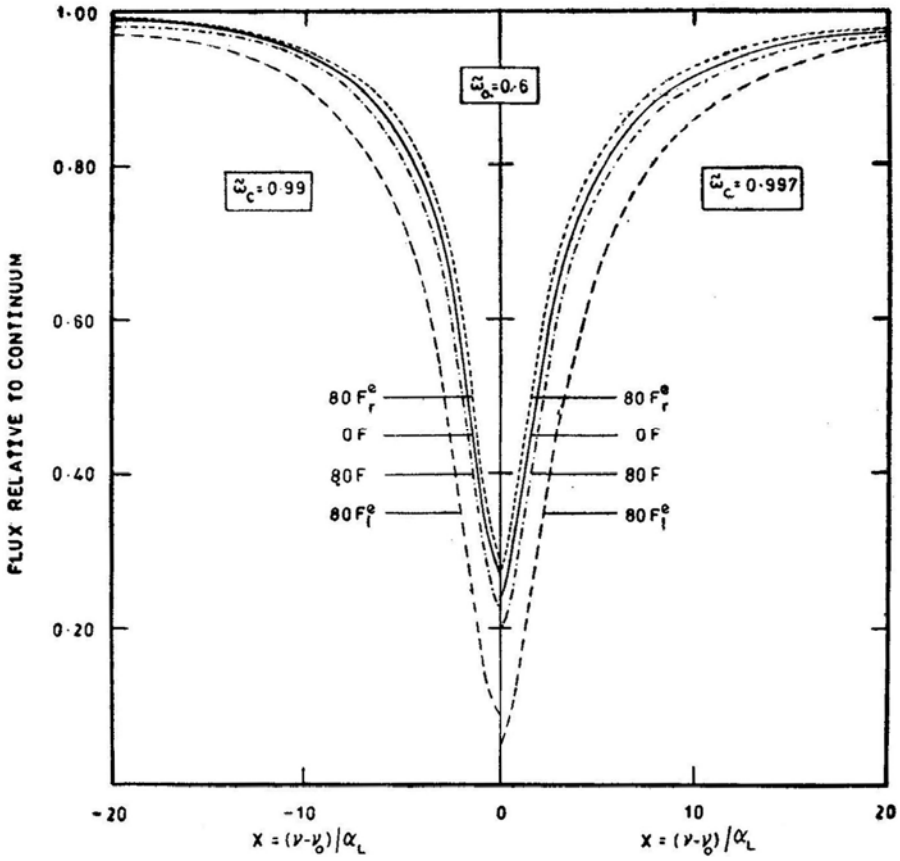

Figure 7. The effect of varying the continuum albedo on the F, F_l^e and F_r^e profiles at two phase angles of 0° and 80° ($\tilde{\omega}_0 = 0{\cdot}6$).

the line becomes weaker, more number of scatterings take place in its formation. Consequently, photons penetrate deeper into the atmosphere and therefore the weakest line shows the maximum change [Young and Kattawar (1976) found the change to be independent of line strength, when they considered a finite atmosphere with Rayleigh's phase function]. Therefore, to sample deeper layers of the atmosphere, one should use the weakest F_l^e lines, which are, however, difficult to observe.

We have repeated the calculations with $\tilde{\omega}_c = 0{\cdot}997$ and $\tilde{\omega}_c = 0{\cdot}999$; while there is not much change in the ratio in the region $0 \leqslant \alpha \leqslant 100$, the decrease in the relative equivalent widths in the remaining region becomes sharper as we go from $\tilde{\omega}_c = 0{\cdot}99$ to $\tilde{\omega}_c = 0{\cdot}999$.

5.2 *The Curves of Growth*

Fig. 10 shows the curves of growth for the total flux F for the following phase angles: 0, 80, 120, 135, 150 and 175 degrees. The transition from the linear to the square-root part is clearly visible in all the curves, the transition being sharper as we approach the phase of 90° where the absorption is maximum. As the absorption becomes

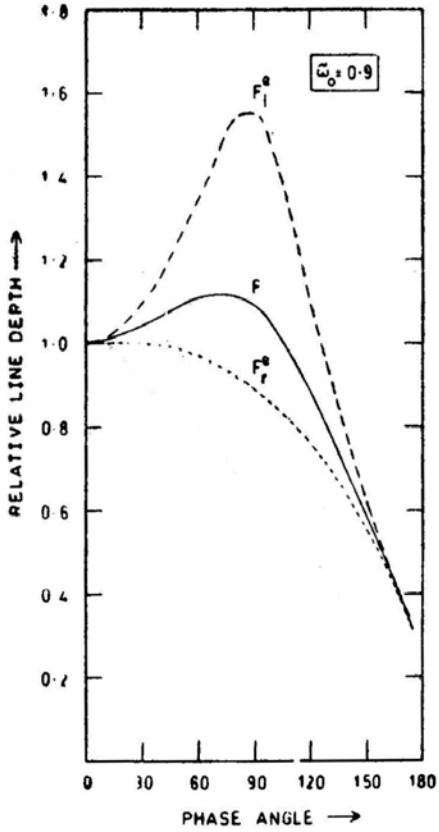

Figure 8. The variation of relative line depth with phase angle for F, F_l^e and F_r^e ($\tilde{\omega}_0 = 0.9$).

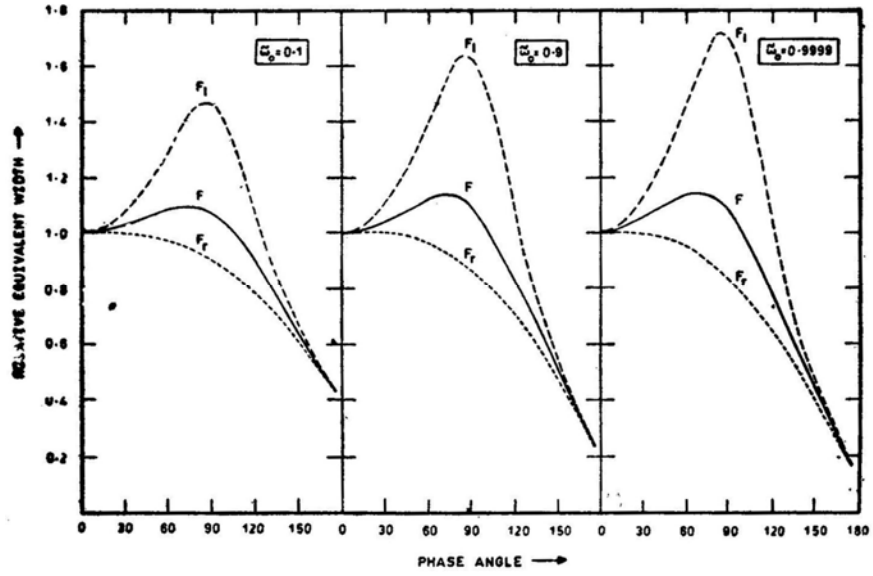

Figure 9. The variation of relative equivalent width with phase angle for F, F_l^e and F_r^e profiles ($\tilde{\omega}_0 = 0{\cdot}1$, $0{\cdot}9$ and $0{\cdot}9999$).

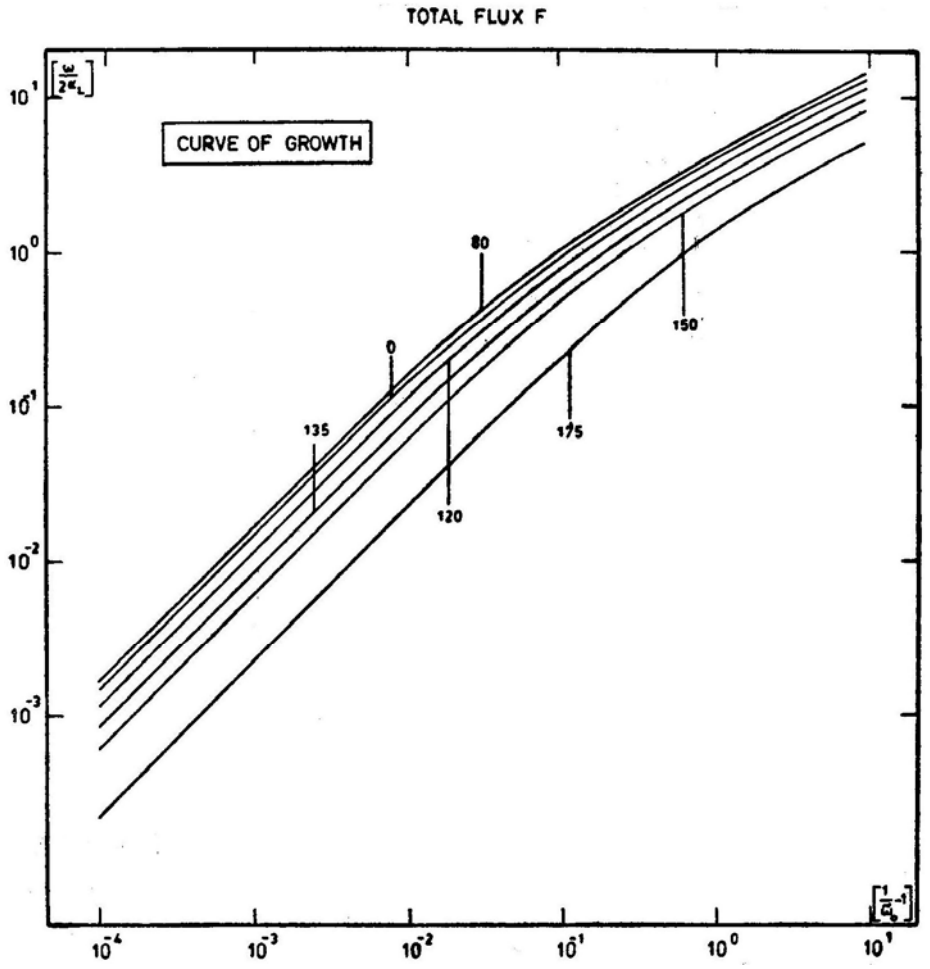

Figure 10. The curve of growth at he different phase angles.

weaker at other phase angles, the extent of the linear portion of the curve of growth increases.

6. Polarization line profiles

The polarization line profiles are shown in Figs 11 and 12 for all the three cases mentioned earlier. The profiles are shown for all the phase angles except 0° and 175° which will be discussed separately. From the two figures it is seen that maximum polarization occurs at line centre and decreases towards the wings, *i.e.* as we approach the continuum, where the values we have computed approach that of Horak (1950) for albedo $\tilde{\omega}_0 = 1{\cdot}0$. The polarization profiles at phase angles 80° and 100° match very closely at the centre but there is a discernible difference towards the wings. A similar behaviour is exhibited at angles 60° and 120° except that the curve at 60° starts above the curve at 120° and falls below as we go from the centre outwards. Thus there is a small asymmetry in the variation of polarization with

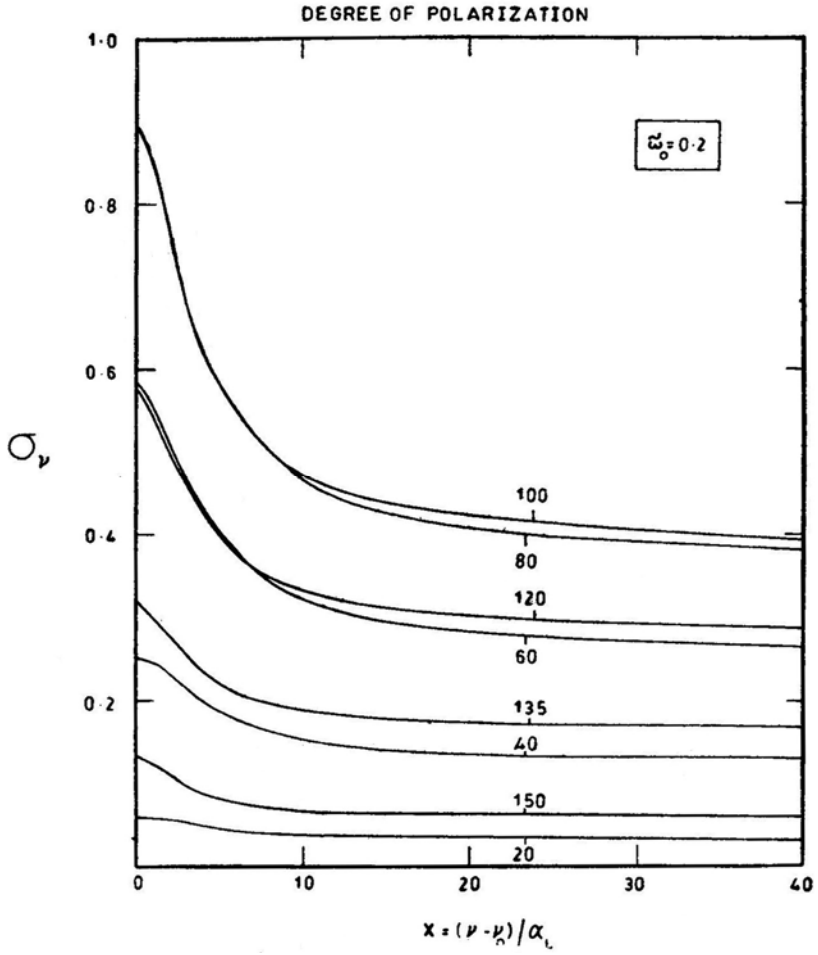

Figure 11. Polarization line profiles at different angles ($\tilde{\omega}_0 = 0.2$).

phase angle which becomes more pronounced towards the wings where the albedo is higher. Fig. 13 shows the asymmetry for three values of the albedo, in which the curve for $\tilde{\omega} = 1$ is due to Horak (1970, personal communication). This can be explained as follows: the polarization in the case of Rayleigh scattering is symmetrical around a scattering angle of 90° for single scattering; this is essentially what we observe at the line centre where the effective number of scatterings is small due to higher absorption. As we go from the line centre to the wings, the effects of multiple scattering predominate which produce increasing asymmetry. Multiple scattering can also be invoked to explain the decrease in polarization towards the wings: it 'scrambles' the initial (high) polarization carried by the lower orders of scattering.

It should also be noted that polarization increases as we go from a weaker ($\tilde{\omega}_0 = 0{\cdot}6$) to a stronger ($\tilde{\omega}_0 = 0{\cdot}2$) line. This is to be expected because the effective number of scatterings at any particular frequency in the line decreases as the line becomes stronger. We have confirmed this by performing calculations for $\tilde{\omega}_0 = 0{\cdot}1$.

Polarization profiles for phase angle 0° and 175° merit separate discussion because the situation here is more complex as shown in, Table 1. At phase angle 0°, the

Table 1. Polarization profiles for extreme phase angles.

ϖ	$X = (\nu-\nu_0)/\alpha_L$			Degree of polarization	
	$\varpi_\theta = 0{\cdot}2$	$\varpi_0 = 0{\cdot}6$	$\varpi^0 = 0{\cdot}9$	$\alpha = 0°$	$\alpha = 175°$
0·1				0·6894 (−05)*	0·2079 (−02)
0·2	0·0503			0·1640 (−04)*	0·2588 (−03)
0·4	1·2980			0·3882 (−04)*	0·3675 (−02)*
0·6	2·2566	0·1240		0·6761 (−04)*	0·8112 (−02)*
0·7	2·9255	0·7701		0·8408 (−04)*	0·1057 (−01)*
0·8	3·9590	1·3338		0·1000 (−03)*	0·1323 (−01)*
0·9	6·2129	2·3664	0·3162	0·1121 (−03)*	0·1614 (−01)*
0·93	7·7705	3·0381	0·8396	0·1129 (−03)*	0·1706 (−01)*
0·95	9·6462	3·8308	1·2698	0·1123 (−03)*	0·1767 (−01)*
0·96	11·2125	4·4855	1·5875	0·1110 (−03)*	0·1797 (−01)*
0·97	13·8224	5·5669	2·0821	0·1095 (−03)*	0·1826 (−01)*
0·98	19·6743	7·9800	3·1273	0·1058 (−03)*	0·1854 (−01)*
0·99	∞	∞	∞	0·1004 (−03)*	0·1878 (−01)*

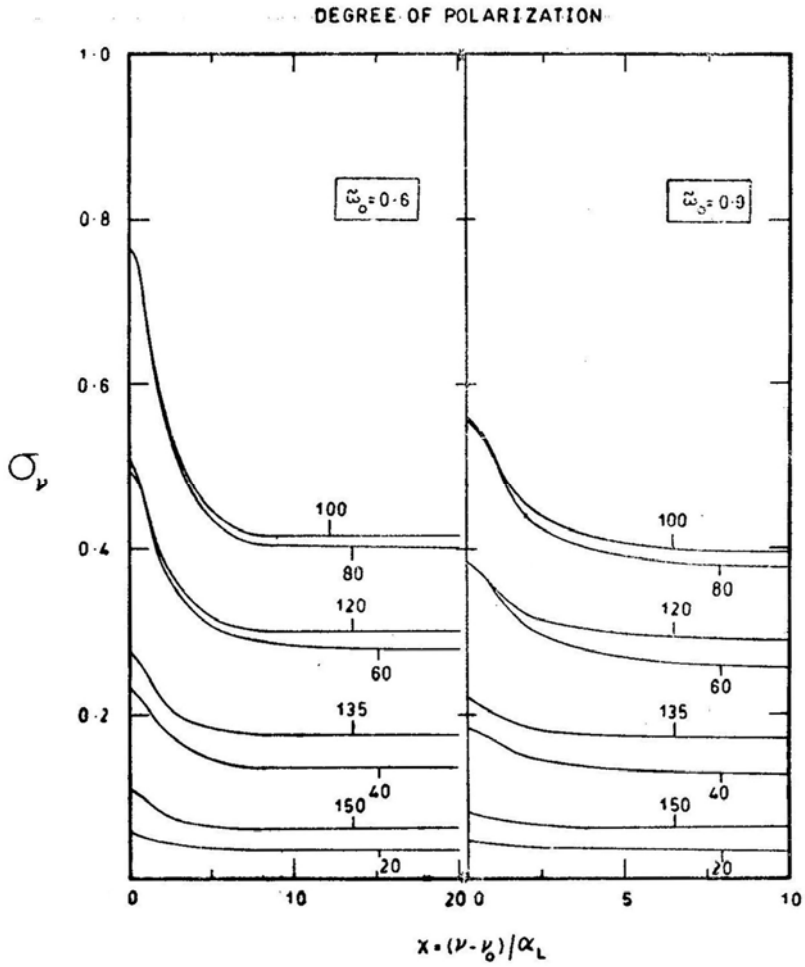

Figure 12. polarization line profiles at different phase angles ($\tilde{\omega}_0$ = 0·6 and 0·9). Note the difference in the scales of abscissa for the two cases.

polarization at line centre for the case $\tilde{\omega}_0$ = 0·2 is small with the F_r^e component less than F_l^e component, and *increases* as we go outwards till the frequency corresponding to albedo 0·93, and then decreases slightly in the extreme wings. For phase angle 175°, again confining our discussion to a line of strength $\tilde{\omega}_0$ = 0·2, we note that the F_r^e component becomes less than the F_l^e component (starred quantities) at a frequency around that corresponding to albedo 0·4. However, in this case there is no decline in polarization in the extreme wings. Further, if we were to consider a line for which $\tilde{\omega}_0$ = 0·1 we would find first a decrease and then an increase in polarization. This upsets the simple picture that multiple scattering always decreases the degree of polarization. It is noteworthy that in both these cases the degree of polarization is small. It seems that if the initial degree of polarization carried by the lower orders of scattering is low, multiple scattering might actually increase the degree of polarization. The Monte-Carlo method or computations of polarization carried by successive orders of scattering can be used to test this theoretically. Calculations to see what Mie-scattering models predict are under way. Further, the

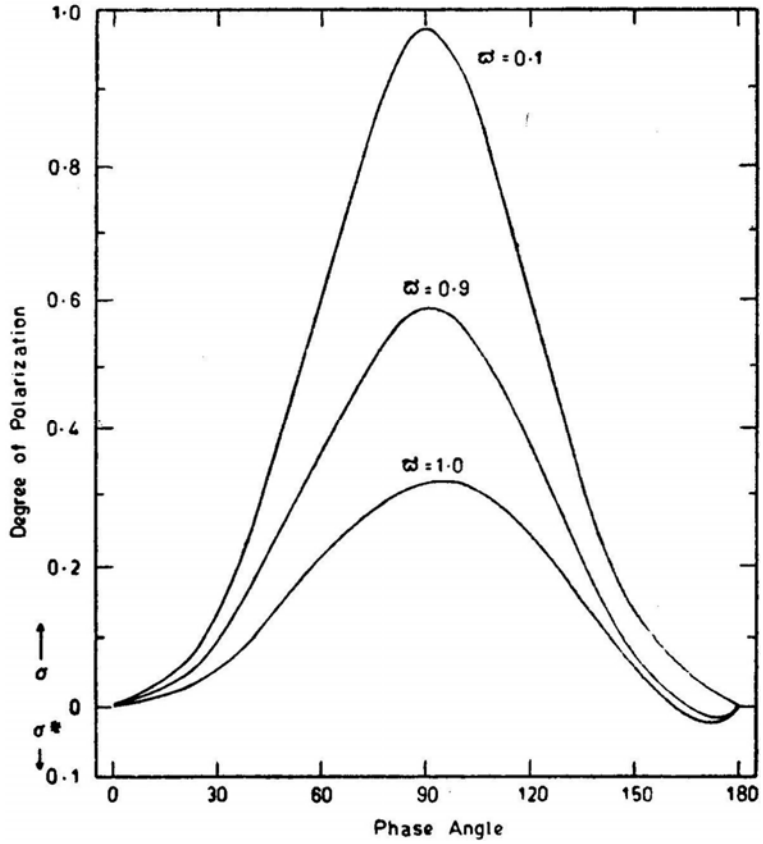

Figure 13. Variation of the degree of polarization of the phase angle for three values of the albedo.

sphericity of the atmosphere has to be taken into account for calculations near phase angle 180°.

It is interesting to note the fact that polarization can increase with albedo already existed in Fig. 8 of Abhyankar and Fymat (1970 a,b), although its significance was not recognized. That the polarization decreased in the extreme wings at $\alpha = 0$ was deduced from the above figure by van de Hulst (1980) who performed the order of scattering calculations for one case corresponding to $\mu = \mu_0 = 0{\cdot}5$ to determine the polarization carried by various orders. He found that the fourth-order scattering carried the maximum polarization.

At present there are no observations against which these results can be checked. Wolstencroft and Smith (1979) have presented some observations of polarization profiles, but they are at a low resolution. With modern detectors, it should be possible to obtain spectra at different phase angles with a polaroid in front of the slit, from which we can get polarization profiles. Alternatively, Fourier transform spectroscopy can be used.

A similar behaviour for points in the disk has been reported elsewhere (Bhatia and Abhyankar 1981). Analysis of the variations of the polarization with albedo at the points of integration for phase angle 0° shows that at some points there is an increase

of polarization with albedo and at some other points a decrease. In the integrated flux, however, there is a decrease. For the phase angle 175° all the points of integration show an increase of polarization with albedo. A detailed analysis of variation on the disk will be published in another paper of the series.

The question remains open: Is the phase effect due to an inhomogeneous atmosphere or due to the phase matrix or both? If it is due to the phase matrix what is the relative importance of Mie and Rayleigh scattering? Further observations having high spectral, spatial and temporal resolution are necessary to decide these questions.

Acknowledgement

R. K. B. would like to thank the University Grants Commission, New Delhi, for the award of a fellowship.

References

Abhyankar, K. D., Fymat, A. L. 1970a, *Astr. Astrophys.*, **4,** 101.
Abhyankar, K. D., Fymat, A. L. 1970b, *Astr. Astrophys.*, **5,** 491.
Abhyankar, K. D., Fymat, A. L. 1971, *Astrophys. J. Suppl. Ser.*, **23,** 35.
Anikonov, A. S. 1977, *Soviet Astr.*, **21,** 95.
Barker, E. S., Macy, W. W. Jr. 1977, *Icarus*, **30,** 551.
Belton, M. J. S. 1968, *J. atmos. Sci.*, **25,** 596.
Bhatia, R. K., Abhyankar, K. D. 1981, *Bull. astr. Soc. India*, **9,** 181.
Bhatia, R. K., Abhyankar, K. D. 1982, *Proc. Indo-U.S. Workshop on High Resolution Spectroscopy*, Bombay.
Buriez, J. C., de Bergh, C. 1980, *Astr. Astrophys.*, **83,** 149.
Buriez, J. C., Fouquart, Y., Fymat, A. L. 1979, *Astr. Astrophys.*, **79,** 287.
Chamberlain, J. W. 1970, *Astrophys. J.*, **159,** 137.
Chamberlain, J. W. 1978, *Theory of Planetary Atmospheres*, Academic Press, New York.
Chandrasekhar, S. 1960, *Radiative Transfer*, Dover, New York,
Clarke, D. 1974, in *Planets*, *Stars and Nebulae*, Ed. T. Gchrels, University of Arizona Press, Tucson p. 45.
Dollfus, A. 1961, in *Planets and Satellites*, Eds G. P. Kuiper and B. M. Middlehurst, University of Chicago Press, p. 343.
Fymat, A. L. 1974, in *Planets*, *Stars and Nebulae*, Ed. T. Gehrels, University of Arizona Press, Tucson, p. 617.
Hansen, J. E., Hovenier, J. W. 1974, *J. atmos. Sci.*, **31,** 1137.
Horak, H. G. 1950, *Astrophys. J.*, **112,** 445.
Hunt, G. E. 1972, *J. quantit. Spectrosc. radiat. Transfer*, **12,** 405.
Hunt, G. E. 1973, *Icarus*, **18,** 637.
Kattawar, G. W., Young, L. D. G. 1977, *Icarus*, **30,** 179.
Lenoble, J. 1968, *J. quantit. Spectrosc. radiat. Transfer*, **8,** 641.
Lenoble, J. 1970, *J. quantit. Spectrosc. radiat. Transfer*, **10,** 533.
Lestrade, J. P., Chamberlain, J. W. 1978, *Icarus*, **34,** 52.
Lestrade, J. P., Chamberlain, J. W. 1980, *Icarus*, **44,** 813.
Macy, W. Jr., Trafton, L. 1977, *Icarus*, **32,** 27.
Michalsky, J. J., Stokes, R. A., Avery, R. W., DeMarcus, W. C. 1974, *Icarus*, **21,** 55.
Regas, J. L., Boese, R. W., Giver, L. P., Miller, J. H. 1973. *J. quantit. Spectrosc. radiat. Transfer*, **13**, 461.
Regas, J. L., Giver, L. P. Boese, R. W ., Miller, J. H. 1975, *Icarus,* **24,** 11.

Sato, M., Kawabata, K., Hansen, J. E. 1977, *Astrophys. J.*, **216,** 947.
Schorn, R. A., Young, A. T., Young, L. D. G. 1979, *Icarus*, **38,** 411.
Teifel, V. G. 1976, in *Jupiter*, Ed. T. Gehrels, University of Arizona Press, Tucson, p. 441.
van de Hulst, H. C. 1980, *Multiple Light Scattering*, Academic Press, New York..
Whitehill, L. P., Hansen, J. E. 1973, *Icarus*, **20,** 146.
Wolstencroft, R. D., Smith, R. J. 1979, *Icarus*, **38,** 155.
Young, L. D. G. 1972, *Icarus*, **17,** 632.
Young, L. D. G., Kattawar, G. W. 1976, *Icarus*, **29,** 483.
Young, L. D. G., Schorn, R. A. J., Young, A. T. 1980, *Icarus*, **41,** 309.